Journal of Solid State Chemistry 182 (2009) 821–826

Contents lists available at ScienceDirect

Journal of Solid State Chemistry

journal homepage: www.elsevier.com/locate/jssc

Crystal structure, magnetic and infrared spectroscopy studies of the $LiCr_yFe_{1-y}P_2O_7$ solid solution

Hssain Bih [a], Ismael Saadoune [a,*], Helmut Ehrenberg [b,c], Hartmut Fuess [b]

[a] Equipe de Chimie des Matériaux et de l'Environnement, FST Marrakech, University Cadi Ayyad, BP549, Av. A. Khattabi, Marrakech, Morocco
[b] Institute for Materials Science, University of Technology, Petersenstr. 23, 64287 Darmstadt, Germany
[c] IFW Dresden, Institute for Complex Materials, Helmholtzstr. 20, 01069 Dresden, Germany

ARTICLE INFO

Article history:
Received 19 September 2008
Received in revised form
3 January 2009
Accepted 7 January 2009
Available online 19 January 2009

Keywords:
Diphosphate
Crystal structure
Magnetization
Infrared spectroscopy

ABSTRACT

The lithium double diphosphates $LiCr_yFe_{1-y}P_2O_7$ have been investigated by X-ray diffraction, SQUID measurements and vibrational spectroscopy. The Rietveld refinements based on the XRD patterns show the existence of a continuous solid solution over the whole composition range ($0 \leqslant y \leqslant 1.0$) with a continuous evolution of the monoclinic unit cell parameters (S.G. $P2_1$). The transition metal ions connect the diphosphate anions forming a three-dimensional network with channels filled by Li^+ cations expected to exhibit high mobility. All compounds order magnetically at low temperatures due the Fe–Fe interactions. The ordering temperature decreases with increasing Cr content. The slope in Curie–Weiss fits to the $1/\chi$ vs T data in the paramagnetic domain clearly shows the existence of Fe^{3+} and Cr^{3+} in their high spin states, and a ferromagnetic component is clearly detected for $y = 0$, 0.2 and 0.4. IR spectra have been interpreted using factor group analysis. The small shift of the frequencies is due to the influence of the chromium amount. The POP angles were estimated using the Lazarev's relationship.

1. Introduction

The use of layered transition-metal oxides as positive electrode materials for lithium secondary batteries has been studied extensively [1–3]. However, for economic and environmental reasons, an alternative class of positive electrode materials based on three-dimensional opened-frameworks, especially those containing PO_4 polyanions, has attracted considerable attention in the last decade [4–6]. Among them, lithium pyrophosphates $LiMP_2O_7$ (M: transition metal) have been subjected to intense research for the past few years, mainly due to the high mobility of lithium ions which promotes the insertion/extraction reactions. Indeed, there are a large number of crystalline materials containing P_2O_7 groups in the literature with the general formula $LiMP_2O_7$. These phosphates exist in different structures: $LiVP_2O_7$ [7], $LiFeP_2O_7$ [8], $LiCrP_2O_7$ [9] crystallize in the space group $P2_1$. In the case of $LiFeP_2O_7$, lithium could be inserted (Fe^{3+} reduction) at 2.95 V against Li/Li^+. Nevertheless, the extraction of lithium from $LiFeP_2O_7$ [10] takes place at high potentials as a result of the high oxidizing power of the Fe^{4+}/Fe^{3+} redox couple. The use of $LiCr_yFe_{1-y}P_2O_7$ as positive electrode materials seems to be a convenient way to reduce the oxidation potential which is essential for electrolyte stability.

In this paper, we first present the preparation and crystal structure analysis of the solid solution $LiCr_yFe_{1-y}P_2O_7$ using Rietveld refinements based on X-ray diffraction data and Infrared spectroscopy (IR spectroscopy). In order to characterize the oxidation state of the transition metal ions and the nature of the magnetic interaction in this type of material, magnetizations of $LiCr_yFe_{1-y}P_2O_7$ with $y = 0$, 0.2, 0.4, 0.6 and 0.8 have been measured down to low temperatures.

2. Experimental

Instead of using solid–solid reactions, we have developed a "wet" method by reaction in an aqueous medium. This type of synthesis leads usually to the formation of solids having higher surface area and/or porosity. An aqueous solution containing a stoichiometric mixture of $Fe(NO_3)_3 \cdot 9H2O$, $Cr(NO_3)_3 \cdot 9H_2O$, $(NH_4)_2HPO_4$ was slowly dripped into LiOH solution. The pH was adjusted to 8 by using an aqueous solution of NH_4OH (1M). The obtained precipitate was first dried under vacuum at 80 °C for 3 h and then dried in air at 120 °C overnight. The calcination of the resulting solid is performed in two steps; the first at 400 °C to decompose the residual nitrates and the second, after grinding, at 750 °C for 12 h.

X-ray diffraction patterns of the powdered samples were obtained with a STOE STADI/P diffractometer (Mo-K_{α_1} radiation, curved Ge (111) monochromator, transmission mode, data step

* Corresponding author. Fax: +212 24 43 31 70.
E-mail address: saadoune1@yahoo.fr (I. Saadoune).

0022-4596/$ - see front matter © 2009 Elsevier Inc. All rights reserved.
doi:10.1016/j.jssc.2009.01.005

width 0.02° (2θ), linear PSD counter). The structures were refined by Rietveld analyzes using the Winplotr package [11].

The magnetic properties of $LiCr_yFe_{1-y}P_2O_7$ samples have been studied with a superconducting quantum interference device (SQUID) from Quantum Design. Measurements were performed upon heating in field cooled (FC) and zero-field cooled (ZFC) mode over the temperature range from 1.8 to 350 K and at constant temperature in field strengths up to 5.5 T.

The infrared measurements were performed in a transmission geometry using a FTIR Biorad spectrometer FTS-40A with dynamic alignment and a spectral resolution of 2 cm^{-1} in the 400–4000 cm^{-1} frequency range; 0.2 mg sample per 200 mg KBr (1 wt%) have been pressed into pellets. Wave number accuracy is within $\pm 2\,cm^{-1}$ for narrow bands.

3. Results and discussion

3.1. Crystal structure

In the whole composition range $0 \leqslant y \leqslant 1.0$, single phases with a color depending on the chromium amount were obtained. In fact, the pristine color of $LiFeP_2O_7$ becomes progressively green as a Cr concentration increases in the studied phosphate. The XRD patterns exhibited very narrow reflections and can all be indexed in the monoclinic system (S.G. $P2_1$).

Fig. 1 gives the evolution of the X-ray patterns of various $LiCr_yFe_{1-y}P_2O_7$ compositions. The similarity of the XRD patterns (peak positions) is an indication of only small variations of the unit cell parameters. The small difference in size between Cr^{3+} and Fe^{3+} [12] and the open and flexible framework of the studied phosphates are the main reason.

In order to elucidate the effect of chromium substitution on the structural features of $LiFeP_2O_7$, its crystal structure was compared in detail with the one for $LiCr_{0.2}Fe_{0.8}P_2O_7$. Both structures were refined based on the initial atomic positions found by Riou et al. from single crystal X-ray diffraction [8].

The observed and calculated XRD patterns together with their difference curves are shown in Fig. 2 for the two selected compositions $LiCr_{0.2}Fe_{0.8}P_2O_7$ and $LiFeP_2O_7$. The results of the Rietveld refinements are summarized in Table 1, and some selected interatomic distances are reported in Table 2.

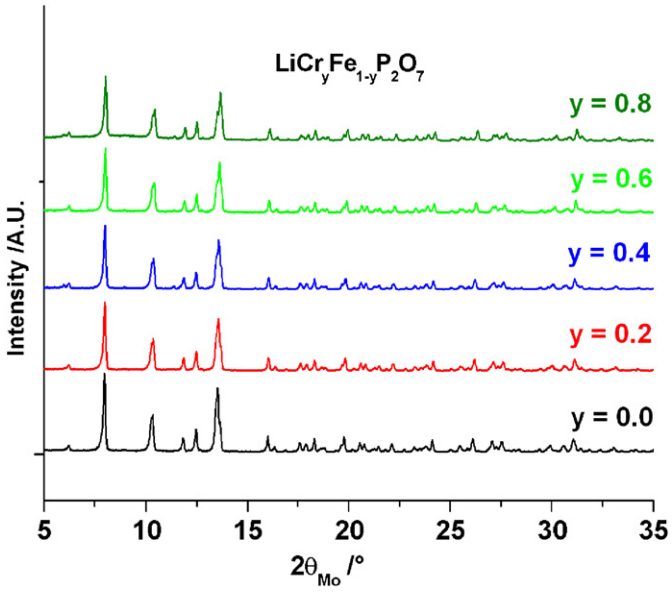

Fig. 1. X-ray diffraction patterns of the $LiCr_yFe_{1-y}P_2O_7$ diphosphates.

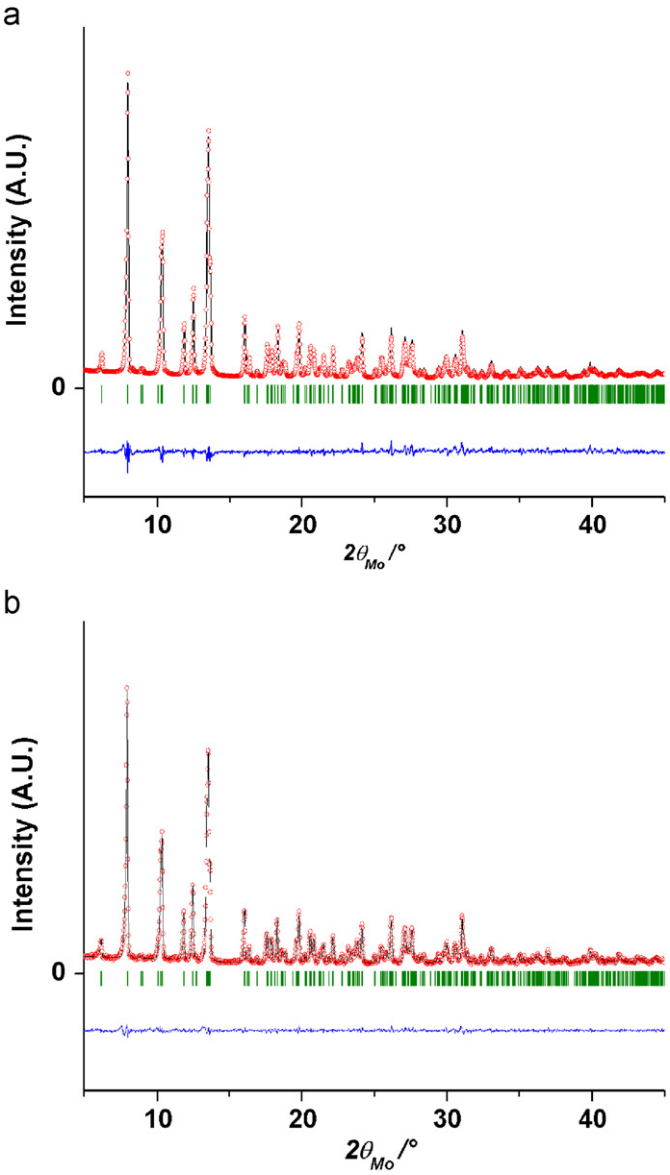

Fig. 2. Final plots of the Rietveld refinement given the comparison of the experimental (•) with the calculated (—) XRD patterns of: (a) $LiFeP_2O_7$ and (b) $LiCr_{0.2}Fe_{0.8}P_2O_7$. Vertical lines refer to the calculated Bragg positions.

The transition metal atoms Cr and Fe have a distorted octahedral environment of oxygen atoms belonging to five P_2O_7 groups. The average *M*–O distance (*M*: Cr, Fe) in $LiFe_{1-y}Cr_yO_2$ varies from 2.022(1) Å for $y = 0$–2.009(2) for $y = 1.0$. This last value is in good agreement with the one reported in the recent X-ray powder diffraction study on $LiCrP_2O_7$ by Ivashkevich et al. [9]. The transition metal cations bridge the diphosphate anions forming a three-dimensional network with channels filled by Li^+ cations. This arrangement is expected to promote a high ionic mobility. In fact, Li^+ ions have a distorted tetrahedral environment of four oxygen atoms belonging to four different P_2O_7 rings. The projection of the studied $LiMP_2O_7$ structure-type along the [100] direction is given in Fig. 3. Note that in the whole composition range, the conformation of the diphosphate group is practically eclipsed and results in bent O–P–O angles of approximately 127°. Furthermore, all distances and angles in the studied diphosphates are in good agreement with many other condensed phosphates reported before [13].

Table 1
Parameters and reliability factors obtained by the Rietveld refinement of the X-ray diffraction pattern of $LiFeP_2O_7$ and $LiCr_{0.2}Fe_{0.8}P_2O_7$.

$LiFeP_2O_7$; space group: $P2_1$ $a = 4.8335(1)$ Å, $b = 8.1014(2)$ Å, $c = 6.9488(5)$ Å $\beta = 109.36(1)^\circ$ $V = 256.7(2)$ Å3, $Z = 2$ Conventional Rietveld factors: $R_p = 10\%$; $R_{wp} = 10.8\%$; $R_B = 3\%$					$LiFe_{0.8}Cr_{0.2}P_2O_7$; space group: $P2_1$ $a = 4.8228(1)$ Å, $b = 8.0790(2)$ Å, $c = 6.9352(3)$ Å $\beta = 109.26(1)^\circ$ $V = 255.1(2)$ Å^3, $Z = 2$ Conventional Rietveld factors: $R_p = 9.5\%$; $R_{wp} = 10.2\%$; $R_B = 2.2\%$				
Atom	Wyckoff	Atomic coordinates			Atom	Wyckoff	Atomic coordinates		
		x	*y*	*z*			*x*	*y*	*z*
Li1	2*a*	0.811(9)	0.382(4)	0.811(9)	Li1	2*a*	0.815(2)	0.387(2)	0.801(7)
Fe1	2*a*	0.2205(6)	0.25	0.2342(1)	Fe/Cr1	2*a*	0.2202(7)	0.25	0.2335(1)
P1	2*a*	0.797(1)	0.4676(2)	0.416(8)	P1	2*a*	0.792(2)	0.4669(9)	0.4147(4)
P2	2*a*	0.602(5)	0.0684(9)	0.9795(4)	P2	2*a*	0.603(8)	0.067(2)	0.9821(3)
O1	2*a*	0.403(3)	0.074(1)	0.112(1)	O1	2*a*	0.403(6)	0.068(5)	0.112(8)
O2	2*a*	0.814(6)	0.219(4)	0.016(1)	O2	2*a*	0.815(1)	0.220(1)	0.023(6)
O3	2*a*	0.134(7)	0.058(9)	0.380(9)	O3	2a	0.125(6)	0.055(5)	0.379(4)
O4	2*a*	0.059(1)	0.429(5)	0.359(4)	O4	2*a*	0.058(8)	0.424(5)	0.356(4)
O5	2*a*	0.249(4)	0.405(8)	0.006(8)	O5	2*a*	0.243(3)	0.407(9)	0.008(5)
O6	2*a*	0.404(4)	0.091(1)	0.744(8)	O6	2*a*	0.410(7)	0.097(8)	0.751(7)
O7	2*a*	0.606(7)	0.322(4)	0.421(3)	O7	2*a*	0.609(6)	0.319(9)	0.423(4)

Table 2
Selected interatomic distances (in Å) for $LiCr_yFe_{1-y}P_2O_7$.

	$y = 0$	$y = 0.2$	$y = 0.4$	$y = 0.6$	$y = 0.8$	$y = 1.0$
(Cr_yFe_{1-y})–O	1.960(2)	1.959(1)	1.927(2)	1.968(1)	1.933(2)	1.971(1)
(Cr_yFe_{1-y})–O	1.986(1)	1.970(2)	1.938(1)	1.980(1)	1.980(1)	1.973(1)
(Cr_yFe_{1-y})–O	1.995(3)	1.978(3)	1.962(1)	1.984(1)	2.009(2)	1.977(1)
(Cr_yFe_{1-y})–O	2.012(1)	2.004(1)	2.010(1)	2.038(1)	2.032(1)	2.012(1)
(Cr_yFe_{1-y})–O	2.049(2)	2.017(1)	2.174(1)	2.039(1)	2.034(2)	2.058(2)
(Cr_yFe_{1-y})–O	2.055(1)	2.019(2)	2.232(1)	2.044(1)	2.045(1)	2.062(1)
P1–O	1.466(1)	1.516(1)	1.439(1)	1.505(2)	1.488(1)	1.495(2)
P1–O	1.513(1)	1.534(2)	1.524(1)	1.531(1)	1.516(1)	1.532(1)
P1–O	1.541(2)	1.599(1)	1.576(2)	1.571(1)	1.566(3)	1.563(2)
P1–O	1.584(1)	1.613(1)	1.742(1)	1.574(1)	1.583(1)	1.607(1)
P2–O	1.457(8)	1.496(1)	1.427(1)	1.477(1)	1.497(1)	1.477(1)
P2–O	1.461(2)	1.504(1)	1.499(3)	1.503(3)	1.508(2)	1.504(3)
P2–O	1.490(1)	1.524(2)	1.570(1)	1.528(1)	1.524(1)	1.533(1)
P2–O	1.594(1)	1.618(1)	1.690(1)	1.623(1)	1.619(1)	1.672(1)
Li–O	1.981(2)	1.943(1)	1.936(1)	1.940(1)	1.915(2)	1.938(1)
Li–O	2.017(2)	1.968(1)	1.975(1)	1.986(2)	2.008(1)	2.027(1)
Li–O	2.021(1)	2.069(2)	1.990(2)	2.003(1)	2.051(1)	2.035(2)
Li–O	2.204(1)	2.158(1)	2.321(1)	2.046(1)	2.095(1)	2.111(1)

3.2. Magnetic properties

The temperature dependences of magnetization of $LiFe_{1-y}Cr_yP_2O_7$ are shown in Fig. 4 for $y = 0$, 0.2 and 0.4 in the low-temperature region. Ferromagnetic components are clearly detected for all three compounds from the difference between FC and ZFC data, and the magnetic ordering temperatures decrease with Cr content. To our knowledge, only two papers deal with the magnetic properties of $LiFeP_2O_7$ [8,14]. According to Riou et al., susceptibility measurements evidence an antiferromagnetic behavior with negative paramagnetic Curie–Weiss temperature ($\theta p \approx -73$ K) and a Néel temperature of $T_N \approx 22$ K. Rousse et al. tried to understand this behavior by using neutron diffraction and symmetry analysis [14]: These authors could determine the magnetic structure and have shown that the magnetic moments of the two iron ions in the unit cell are oriented mainly antiparallel to each other along a direction close to the *a*-axis. Accordingly, the magnetic structure corresponds to the representation Γ_1, which allows a ferromagnetic component along the *b*-axis, clearly observed in our study (see Fig. 4) but missed by Riou et al. Three super–super exchange interactions have to be considered to obtain this magnetic structure as the ground state

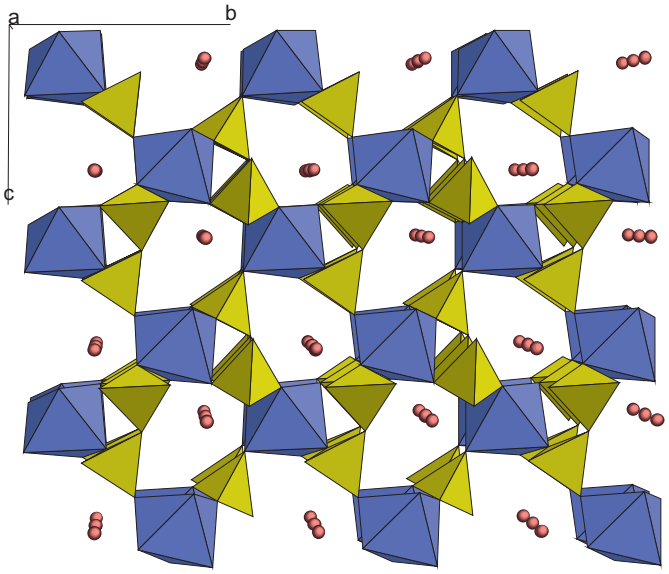

Fig. 3. Crystal structure of $LiCr_yFe_{1-y}P_2O_7$ diphosphates, view along the '*a*' axis. Red circles denote the lithium atoms. (For interpretation of this figure legend, the reader is referred to the web version of this article.)

[14]. The calculated magnetic phase diagram indicates that the exchange interaction along the shortest Fe–Fe distance has to be positive and the two others negative. Furthermore, the magnetic behavior results from the super–super exchange interactions involving two oxygen atoms belonging to one PO_4 tetrahedron.

At higher temperature magnetization versus temperature obeys a Curie–Weiss law, and the derived paramagnetic moments and Curie–Weiss temperatures are summarized in Table 3 from fits to the data above 50 K. The standard deviations in brackets are determined by least-squares fits, and a change of the parameter by the value in brackets results in a 10% higher residual than the minimum. The theoretical value for the $S = 5/2$ state of Fe^{3+} ($\mu_{eff} = 2\sqrt{S(S+1)} = 5.92\,\mu_B$) is in excellent agreement with the observed value $5.94(1)\,\mu_B$ and confirms the high-spin configuration. Chromium substitution for iron reduces the effective magnetic moment μ_{eff} and the Curie–Weiss temperature θ as reported in Table 3, reflecting lower magnetic moments of Cr^{3+}-ions, weaker magnetic interactions between Cr–Fe and Cr–Cr

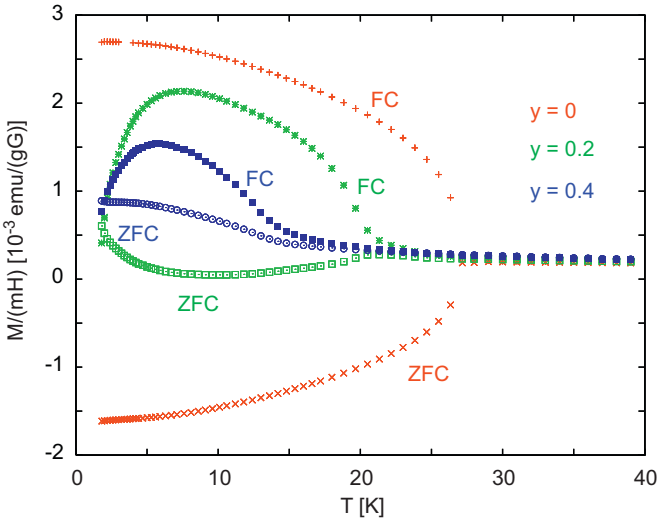

Fig. 4. Specific magnetization per field of $LiCr_yFe_{1-y}P_2O_7$ for $y = 0$, 0.2 and 0.4 in field-cooled (FC) and zero-field cooled mode (ZFC). The applied field strength was 100G.

Table 3
Magnetic properties of $LiCr_yFe_{1-y}P_2O_7$ diphosphates.

y in $LiCr_yFe_{1-y}P_2O_7$	$\mu_{exp.}$ (μ_B)	$\mu_{calc.}$ (H.S) (μ_B)	θ (K)
0	5.94(1)	5.92	−55(1)
0.2	5.49(1)	5.57	−41(1)
0.4	5.20(1)	5.20	−27(1)
0.6	4.68(1)	4.80	−15(1)
0.8	4.27(1)	4.36	−6.5(5)

The effective magnetic moments are calculated based on a spin-only contribution of 3.87 μ_B per Cr^{3+}-ion

ions than between Fe–Fe and, as a consequence, a breakdown of magnetic ordering. This is not surprising, because competing exchange interactions are expected for Fe^{3+} and Cr^{3+}, and a similar behavior was recently observed for the network structures along the solid solution $NaFe_yCr_{1-y}W_2O_8$ [15].

3.3. IR spectroscopy

In all studied compounds, the $P_2O_7^{4-}$ polyhedra have C_{2v} space group. The factor group analysis was performed using the procedure developed by Hamuza and Serghini groups [16,17]. The 21 fundamental vibrations of the $P_2O_7^{4-}$ groups are subdivided as follows:

$$\Gamma_{vib}(C_{2v}) = 7A_1(\mathrm{IR,Ra}) \oplus 4A_2(\mathrm{Ra}) \oplus 6B_1(\mathrm{IR,Ra}) \oplus 4B_2(\mathrm{IR,Ra})$$

The correlation scheme for the internal modes of the $P_2O_7^{4-}$ anions is given in Table 4. Due to the non-centrosymmetric structure with the space group C_{2v}, all Raman-active bands are also allowed and active in the infrared spectra. Thus, according to the selection rules, 42 bands are both infrared and Raman-active. On the other hand, the external vibrations of $LiMP_2O_7$ (M: Fe, Cr) phosphate correspond to rotational motions of $P_2O_7^{4-}$ ions and translational motions of Li^+, M^{3+} cations and $P_2O_7^{4-}$. The correlation scheme predicted 12 translational and 12 rotational modes:

$$\Gamma_{vib(T+R)} = 12A(\mathrm{IR,Ra}) \oplus 12B(\mathrm{IR,Ra})$$

The infrared spectra of the studied compounds are shown in Fig. 5, whereas, their band assignments are summarized in Table 5. The similarity of all these vibrational spectra confirms that all

Table 4
Correlation scheme for the internal modes of $P_2O_7^{4-}$ anions.

Ion	Movement	M_G (C_{2v})	S_G (C_1)	S_G (C_2)
$P_2O_7^{4-}$	Internal vibration	7A1(IR, Ra) 4A2 (Ra)	21A(IR, Ra)	21A(IR, Ra) 21B(IR, Ra)
		4B1(IR, Ra) 6B2(IR, Ra)		

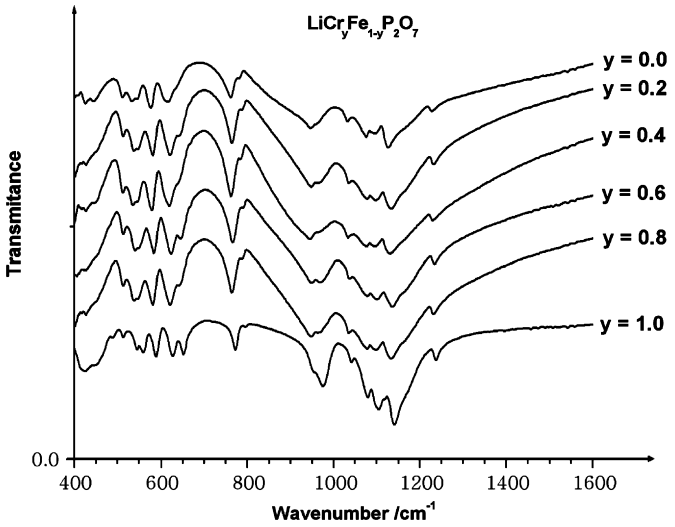

Fig. 5. IR Spectra of $LiCr_yFe_{1-y}P_2O_7$ diphosphate.

Table 5
P–O–P angle values in $LiCr_yFe_{1-y}P_2O_7$ calculated from the Lazarev's relationship.

Composition	ν_{as} POP (cm^{-1})	ν_sPOP (cm^{-1})	100Δ	POP (degree)
$LiFeP_2O_7$	952	762	11.09	124.3
$LiCr_{0.2}Fe_{0.8}P_2O_7$	953	762	11.14	124.9
$LiCr_{0.4}Fe_{0.6}P_2O_7$	955	763	11.18	125.3
$LiCr_{0.6}Fe_{0.4}P_2O_7$	958	765	11.20	125.7
$LiCr_{0.8}Fe_{0.2}P_2O_7$	962	766	11.34	127
$LiCrP_2O_7$	966	769	11.35	127.2

$LiFe_{1-y}Cr_yP_2O_7$ compounds adopt the same crystal structure. The assignment of the observed spectral features of different entities is based on a comparison with structurally related materials [18–20] with the following sequence of pyrophosphate vibrations in the order of decreasing frequency:

$$\nu_{as}(PO_3) > \nu_s(PO_3) > \nu_{as}(POP) > \nu_s(POP) > \delta_{as}(PO_3) > \delta_s(PO_3) > \delta_s(POP)$$

ν_{as} and ν_s refer to asymmetric and symmetric stretching vibrations of the terminal (PO_3) or bridging (POP) bonds, respectively, while δ refers to the corresponding bond binding vibrations, which are in general of lower frequency.

Note that one of the most interesting aspects of this study is the ability to obtain direct information about the configuration of the P–O–P bridges. Furthermore, the symmetric POP bridge stretching mode (ν_sPOP) can be used to confirm the presence of the diphosphate group in the $LiCr_yFe_{1-y}P_2O_7$ solid solution. Indeed, the presence of the symmetric and antisymmetric bridge stretching vibration (around 760 cm^{-1}) in the infrared spectra of the compounds within this series can be considered as a definitive proof of a bent POP bridge configuration.

Table 6
Vibrational spectra data (cm^{-1}) and band assignments in $LiCr_yFe_{1-y}P_2O_7$.

$y=0$	$y=0.2$	$y=0.4$	$y=0.6$	$y=0.8$	$y=1.0$	Assignment
1224 s	1230 s	1231 s	1235 s	1234 s	1237 s	$\nu_{as}(PO_3)$
1126 vs	1132 vs	1133 vs	1137 vs	1133 vs	1105 vs	ν_{as} (PO_3)
1095 vs	1096 vs	1097 vs	1100 vs	1101 vs	1140 vs	ν_{as} (PO_3)
1077 s	1074 s	1075 s	1079 s	1075 s	1082 s	$_{vs}$ (PO_3)
1030 w	1031 w	1032 w	1039 w	1036 w	1039 w	$_{vs}$ (PO_3)
961 s	962 s	964 s	967 s	973 s	975 vs	ν_{as} P–O–P
943 vs	944 vs	946 vs	949 vs	951 vs	957 s	ν_{as} P–O–P
762 s	762 s	763 s	765 s	766 s	769 s	$_{vs}$ P–O–P
634 m	636 m	641 m	649 m	642 m	652 s	δPO_3 and ρPO_3
612 s	618 s	618 s	623 s	620 s	627 s	δPO_3 and ρPO_3
576 s	580 s	581 s	583 s	580 s	587 s	δPO_3 and ρPO_3
543 m	543 m	544 m	551 m	547 m	558 m	δPO_3 and ρPO_3
29 m	532 m	534 m	540 m	540 m	544 m	δPO_3 and ρPO_3
506 w	506 w	508 w	511 w	511'w	515 w	δPO_3 and ρPO_3
441 w	441 w	443 w	428 w	450 w	450 w	δPO_3 and ρPO_3
424 w	423 w	424 w	406 w	423 w	423 m	δPO_3 and ρPO_3

s: strong; vs: very strong; m: medium; and w: weak.

Furthermore, the P–O–P bridge of $P_2O_7^{4-}$ group may be considered as an independently vibrating unit. Within this approximation, its stretching frequencies depend on the POP angle, but also on that of the P–O bond force within the bridge:

$$\nu_S(\mathrm{POP}) = \frac{1}{2}\pi c\sqrt{k\left(\frac{1}{m_p}+\frac{1+\cos\alpha}{m_o}\right)}$$

$$\nu_S(\mathrm{POP}) = \frac{1}{2}\pi c\sqrt{k\left(\frac{1}{m_p}+\frac{1-\cos\alpha}{m_o}\right)},$$

where k is the force constant; m_p the mass of phosphorous atoms; m_o the mass of oxygen atoms and α the P–O–P angle. This approximation leads to the Lazarev's relation [21]:

$$\Delta = (\nu_{as}(\mathrm{POP})\text{-}\nu_s(\mathrm{POP}))/(\nu_{as}(\mathrm{POP}) + \nu_s(\mathrm{POP})) = f(\alpha)$$

This relation does not depend on the force constant. Vibrational studies of pyrosilicates, pyrogermanates and pyrophosphates [22,23] show that the Lazarev's relation is obeyed for numerous compounds. This relation is now applied to the case of $LiCr_yFe_{1-y}P_2O_7$ (Table 6). As shown in Fig. 6, a linear evolution of the POP angle values with the amount of chromium was evidenced. Furthermore, the derived POP angles agree well with those obtained by the Rietveld refinements of the crystal structures.

4. Conclusion

$LiCr_yFe_{1-y}P_2O_7$ diphosphates have been prepared using a wet method at relatively low temperatures and were characterized by X-ray diffraction, magnetization studies and IR spectroscopy measurements. Their structures have been refined based on powder diffraction by the Rietveld method. This study shows the existence of a continuous solid solution with monoclinic symmetry (S.G. $P2_1$). A small evolution of the unit cell parameters is evidenced as a result of the small difference in the ionic radii of the Cr^{3+} and Fe^{3+} ions in a distorted octahedral environment of oxygen atoms, belonging to five different P_2O_7 groups. Lithium ions are situated in a distorted tetrahedral environment, formed by four oxygen atoms belonging to four different P_2O_7 rings. The high-spin configurations of both transition metal ions were concluded from the averaged magnetic moments in the paramagnetic region. The dominant magnetic couplings are antiferromagnetic, reflected in the negative Curie–Weiss temperatures. Substitution of chromium for iron leads to a decrease of the Curie–Weiss temperatures θ_p as a result of weaker M–M' exchange interactions for M or $M' = Cr$ instead of Fe.

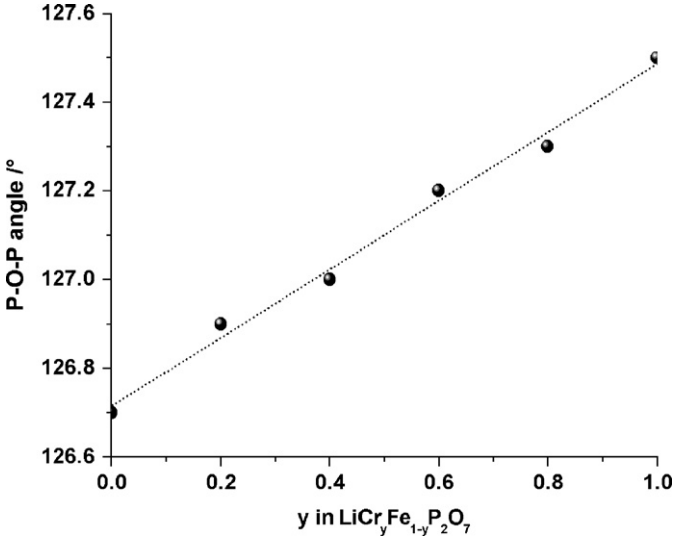

Fig. 6. Evolution of the P–O–P angle value, calculated from the Lazarev's relationship, with the chromium amount.

The infrared spectra of the studied compounds were recorded and interpreted using factor group analysis. The similarities of the vibrational spectra confirm that these condensed phosphates are all isostructural. The spectroscopic data clearly show a bent conformation of the P–O–P bridges in $LiCr_yFe_{1-y}P_2O_7$. The POP bridge angles are derived from Lazarev's relation and agree well with those deduced from the crystal structure refinement.

Acknowledgments

This work has been supported by the CNRST (Morocco)–DFG (Germany) convention (Grant no. 445-MAR-113/18/2).

References

[1] J.R. Dahn, U. von Sacken, M.W. Juzkow, H. Al-Janaby, J. Electrochem. Soc. 138 (1991) 2207.
[2] K. Ozawa, Solid State Ionics 69 (1994) 212.
[3] M. Dahbi, I. Saadoune, J.M. Amarilla, Electrochim. Acta 53 (16) (2008) 5266–5271.
[4] A.K. Padhi, K.S. Nanjundaswamy, J.B. Goodenough, J. Electrochem. Soc. 144 (4) (1997) 1188–1194.
[5] A.S. Andersson, B. Kalska, P. Eyob, D. Aernout, L. Häggström, J.O. Thomas, Solid State Ionics 140 (2001) 63–70.
[6] H. Wang, K. Huang, Y. Zeng, S. Yang, L. Chen, Electrochim. Acta 52 (2007) 3280–3285.
[7] K.H. Lii, Y.P. Wang, Y.B. Chen, S.L. Wang, J. Solid State Chem. 86 (2) (1990) 143–148.
[8] D. Riou, N. Nguyen, R. Benloucif, B. Raveau, Mater. Res. Bull. 25 (1990) 1363.
[9] L.S. Ivashkevich, K.A. Selevich, A.I. Lesnikovich, A.F. Selevich, Acta Cryst. E 63 (2007) i70–i72.
[10] A.K. Padhi, K.S. Nanjundaswamy, C. Masquelier, S. Okada, J.B. Goodenough, J. Electrochem. Soc. 144 (1997) 1609.
[11] J. Rodriguez-Carjajal, Laboratoire Léon Brillouin ⟨http://www.llb.cea.fr/fullweb/powder.html⟩.
[12] R.D. Shannon, Structure and Bonding in Crystals, Academic Press, San Diego, 1981.
[13] A. Durif, Crystal Chemistry of Condensed Phosphates, Plenum Press, New York, 1995.
[14] G. Rousse, J. Rodríguez-Carvajal, C. Wurm, C. Masquelier, Solid State Sci. 4 (2002) 973–978.
[15] L. Nyam-Ochir, H. Ehrenberg, A. Buchsteiner, A. Senyshyn, H. Fuess, D. Sangaa, J. Magn. Magn. Mater. 320 (2008) 3251–3255.
[16] J. Hamuza, B. Jerowska-Tzebiatowska, K. Lukaszewicz, J. Mol. Struct. 13 (1972) 391.
[17] M. Serghini Idrissi, L. Rghioui, R. Nejjar, L. Benarafa, M. Saidi Idrissi, A. Lorriaux, F. Wallart, Spectrochim. Acta 60A (2004) 2043–2052.

[18] N. Santha, V. Nayar, G. Keresztury, Spectrochim. Acta 49A (1993) 47.
[19] V.P. Mahadevan Pillai, B.R. Thomas, V. Nayar, K.H. Lii, Spectrochim. Acta 55A (1999) 1809.
[20] U. Kuhlmann, C. Thomsen, A.V. Prokoviev, F. Büllesfeld, E. Uhrig, W. Assmus, Physica B 301 (2001) 276–285.
[21] A.N. Lazarev, Vibrational Spectra and Structure of Silicates, Consultants Bureau (English Translation), New York, 1972.
[22] M. Gabelica-Robert, Thesis, University of Liege, Belgium, 1981.
[23] M. Harcharras, A. Ennaciri, A. Rulmont, B. Gilbert, Spectrochim. Acta 53A (1997) 345–352.